



Fabrication of novel nanocomposites from styrene-butadiene rubber/zinc sulphide nanoparticles

V. C. Jasna¹ and M. T. Ramesan^{1,*}

¹Department of Chemistry, University of Calicut, Calicut University P.O., Malappuram 673 635, Kerala, India

Received: 24 October 2017

Accepted: 23 February 2018

Published online:
5 March 2018

© Springer Science+Business
Media, LLC, part of Springer
Nature 2018

ABSTRACT

The present study critically investigates the evaluation of zinc sulphide nanoparticles (ZnS) as potential crystalline inclusion in styrene-butadiene rubber (SBR). The prepared nanocomposite was characterized by a Monsanto Rheometer, and the vulcanization was carried out to their respective cure time values. The X-ray diffraction reveals the decrease in the amorphous phase of composite with the addition of ZnS nanoparticles. The uniform morphology of SBR was changed into a non-uniform pattern in the presence of ZnS nanoparticles, and few agglomerations were visible at higher loading of fillers. The effective utilization of the surface of nanoparticles by SBR chains resulted in an enhancement in rheometric torque or viscosities and a reduction in optimum cure and scorch time. Thermal stability studied by thermogravimetry (TGA) showed a remarkable increase in the thermal resistance of composites, and the thermal stability increases with an increase in the concentration of ZnS. The reinforcing natures of ZnS in SBR matrix were evident from increased mechanical properties such as tensile and tear strength, modulus, compression set, hardness and heat build-up behaviours. Effective formation of conductive chains of ZnS nanoparticles at 10 phr loading results in a maximum value of electrical conductivity. The diffusion and transport mechanisms of petroleum fuels through the polymeric membranes were studied according to the concentration of nanoparticles, the effect of solvent and temperature. The mechanism of diffusion shows an anomalous trend. The activation energy of diffusion and permeation of composites was also calculated from the sorption analysis.

Introduction

Over the past years, research in the field of nanoparticles and their composites with polymers has fascinated the scientific paradigm. One of the reasons is the high performance to weight ratio of the

resulting polymer nanocomposites. The reinforcement imparted to the polymers by nanoparticles resulted in a material with improved mechanical properties, flame retardant, air and liquid barrier properties coupled with dimensional and thermal stability [1–5]. They serve as an excellent substitute

Address correspondence to E-mail: mtramesan@hotmail.com

for conventional engineering materials in construction and automotive sectors. Among the broad variety of nanoparticles available for the development of elastomeric nanocomposites, nanoparticles having specific functional groups are of great interest. This is due to their novel properties and versatile applications [6–8].

Elastomers combine the attractive properties of insulation with flexibility. However, a flexible elastomer with high dielectric constant widens their application to charge storage capacitors, electrostriction artificial muscles and novel drug delivery. Metal oxides or metal sulphide nanoparticles being unique dielectric materials, with excellent thermal stability and their addition to polymers, have been carried out to make the polymers thermally more stable and conductive [9, 10]. Flame retardancy, thermal stability and electrical properties such as the AC conductivity, dielectric constant and dielectric loss tangent of a polymeric system depend on the nature and amount of metal nanoparticles [11, 12]. The increase in AC conductivity of such nanocomposites stems from the formation of a continuous conductive chain network of nanoparticles in the polymer matrix. These conductive nanocomposite materials find application in electrostatic discharge devices in electromagnetic interference shielding and in other electronic applications [13–15].

Styrene-butadiene rubber (SBR) is unique in its excellent abrasion resistance, thermal and ageing stability. SBR is a major and unavoidable component of tires, cables, insulating materials, shoe soles and gaskets [16, 17]. However, unfilled SBR has poor tensile strength, flame retardant and oil resistance. The poor tensile strength is due to the absence of strain-induced crystallization and the highly amorphous nature of SBR. The mechanical properties can be improved by the reinforcement of SBR with micro- and nanofiller particles.

Polymer composites are widely used in the construction and automobile industries. In the automobile industry, they serve as oil seals and gaskets. Thermal stability is one of the important properties for the preparation of oil seals [18–20]. During service, if they subjected to excess temperature, the material may undergo thermal degradation and may become soft. Also, the contact of these materials with industrial solvents/fuels results in leakage problems and failure in sealing. Hence, it is necessary to focus more attention on selecting elastomers to prepare

materials which are in contact with industrial solvents such as petrol, diesel and kerosene. The transportation of petroleum fuels through a polymeric membrane is of technological importance in a variety of applications. Even though many studies on the use of montmorillonites as reinforcing nanofiller in polymer matrices have been reported [21, 22], the detailed transport studies on inorganic nanofillers/elastomers are rare.

The main purpose of the present work is to explore the effect of ZnS nanoparticles on the mechanical, thermal, dielectric and solvent transport properties of SBR. To our knowledge, till date, no studies have been reported on the electrical, mechanical properties and the interaction of petroleum fuels with SBR/ZnS nanocomposite. The present study deals with the development of a new class of SBR/ZnS nanocomposites through a simple, inexpensive two roll mill mixing technique. This study investigates in detail the cure characteristics, morphology, transport behaviour, dielectric and the mechanical properties with respect to the different contents of nanoparticles.

Experiment

Materials and methods

SBR (Synaprene 1502) was procured from Synthetics and Chemicals Ltd., India. Cetyl trimethyl ammonium bromide (CTAB), zinc sulphate and sodium sulphide were purchased from HiMedia chemicals. The solvents like petrol (mol. wt. 100), kerosene (mol. wt. 170) and diesel (mol. wt. 230) were of reagent grade procured from Bharat Petroleum Corporation Limited, India. Rubber ingredients such as stearic acid, zinc oxide (ZnO), cyclohexyl benzothiazole (CBS), 2,2,4-trimethyl-1,2-dihydroquinoline (TDQ), processing oil and sulphur were obtained from local chemical suppliers.

Preparation of zinc sulphide nanoparticles

ZnS nanoparticles were prepared using a hydrothermal method [23]. An equimolar ratio of $\text{ZnSO}_4 \cdot 5\text{H}_2\text{O}$ and $\text{Na}_2\text{S} \cdot 7\text{H}_2\text{O}$ powder was dissolved separately in de-ionized water. The sodium sulphide solution was then added drop-wise to the ZnSO_4 solution with constant stirring. The white precipitate formed was charged into the Teflon-lined stainless

steel autoclave and maintained in an ambient pressure at a temperature of 220 °C for 12 h. It was then allowed to cool naturally. The washing procedure was repeated several times to remove impurities from the sample. The precipitated sample was first washed with de-ionized water followed by alcohol to remove impurities. It was dried at 60 °C in a vacuum oven for 12 h.

Preparation of SBR/ZnS nanocomposites

The compounding of SBR with different amounts of ZnS nanoparticles (0, 3, 5, 7, 10 and 15 parts per 100 parts rubber (phr)) was done in a two roll mixing mill. The basic formulation used for the preparation of nanocomposite is as follows: 5.0 (phr) ZnO, 2.0 (phr) stearic acid, 1.0 (phr) TDQ, processing oil 1/20th of filler, 1.2 (phr) CBS and 2.4 (phr) sulphur. The mixing was done at 28 °C as per the ASTM D-15-627 (1994) method, with special attention to ensure the uniform distribution of filler particles. The samples were named as SZ₀ for SBR with no filler loading. SZ₃, SZ₅, SZ₇, SZ₁₀ and SZ₁₅ are composites with 3, 5, 10 and 15 (phr) of ZnS nanoparticles.

Characterization techniques

The X-ray diffraction analysis of the composite materials was studied using a Bruker AXS D X-ray diffractometer with CuK α radiation ($\lambda = 1.5406 \text{ \AA}$) with an accelerating voltage of 30 kV. The diffractograms were recorded in the range of $2\theta = 10^\circ\text{--}80^\circ$ at a speed rate of 2° min^{-1} . The surface morphology of the fabricated polymer nanocomposites was analysed by a Hitachi S-3000 H scanning electron microscope. For SEM analysis, the rubber compounds were immersed in liquid nitrogen for 5 min and then fractured. These samples were mounted on the stubs, and the rubber surface was sputtered with platinum-palladium to resist the charging on the surface before examining under SEM. Electrical properties of the samples were measured by using the vulcanized sheet (circular shape of 0.3–0.5 mm thick, 1.2 cm diameter). The thermal stability of the nanocomposite was analysed by Perkin-Elmer thermogravimetric analyser (TGA) at a heating rate of $10^\circ \text{ C min}^{-1}$ in a nitrogen atmosphere. The AC conductivity and dielectric loss of SBR nanocomposites were measured by an automatic Hewlett Packard LCR metre (HP, 4284A) in the frequency range of $10^2\text{--}10^6 \text{ Hz}$. The

cure characteristics of the mixes were followed by using a Monsanto Rheometer R-100 at a rotational frequency of $100 \text{ cycles min}^{-1}$ as per ASTM standard D-5289 (2001) at 150 °C. The moulding of samples was done in a hydraulic press at 40 MPa pressures as per the corresponding optimum cure time obtained from Rheometer. The tensile strength and tear resistance of the dumb-bell-shaped samples were tested in a Zwick universal testing machine (UTM) at 28 °C and at a cross head speed of 500 mm min^{-1} according to ASTM D 412 (2016) and ASTM D 624-00 (2012), respectively. The hardness of composites was measured at room temperature by using a Shore-A hardness tester (Durometer-Mitutoyo Shore-A metre) as per ASTM D-2240 (1999). The samples having a thickness of 6 mm were used for this study. The instrument used a calibrated spring to provide the indenting force. The load imposed by the spring varied with indentation. Using the constant strain method by keeping the vulcanized compound at 70 °C for 22 h, according to ASTM D 395-(2016) method B, the compression set values were studied. The heat build-up of SBR vulcanizate and SBR/ZnS nanocomposite vulcanizate was determined by a Goodrich flexometer according to ASTM D 623 (2007). Applying DIN EN ISO 5470-1 procedure in DIN abrader, the abrasion resistance of the composites was measured. The solvent imbibing and transport properties of SBR/ZnS nanocomposites were tested by cutting circle-shaped samples from the vulcanized sheets. The diffusion and transport of petroleum fuels in SBR and SBR/ZnS nanocomposite vulcanizates were studied gravimetrically using circular disc-like samples, taking the increase in weight at regular interval of time. The same experiment was conducted at different temperatures also [24].

Results and discussion

X-ray diffraction analysis (XRD)

The XRD pattern of ZnS, SBR and SBR/ZnS nanocomposites is displayed in Fig. 1. The XRD of ZnS (Fig. 1e) shows the 2θ values at 28.79° , 48.23° and 56.97° which are the corresponding crystal plane of (111), (220) and (311), respectively, of the cubic phase of ZnS matching with JCPDF 80-0020 [23, 24]. The XRD peaks are broadened due to the nanocrystalline nature of the synthesized ZnS. No additional peaks

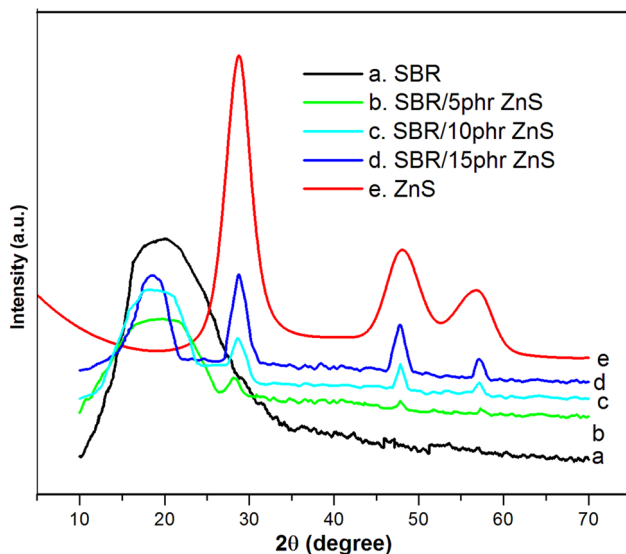


Figure 1 XRD pattern of ZnS, SBR and different contents of ZnS-filled SBR.

are detected for impurities in the sample confirming the phase purity of the synthesized ZnS nanoparticles. The average crystallite size of the powder has been estimated automatically from corresponding XRD data using Scherrer formula, $D = 0.94\lambda/\beta \cos\theta$, and the average crystallite size is 2.9 nm. SBR shows a broad peak at $2\theta = 20.17^\circ$ indicating its amorphous nature. It is evident from the figure that the amorphous peak of composites is slightly shifted to a lower diffraction angle with a decrease in the broadness of the peak than that of the corresponding position in pure SBR. For example, the diffraction of 15 phr composite is slightly shifted to a lower diffraction angle from $2\theta = 20.17^\circ$ – 18.76° . The decrease in amorphous nature of SBR with the shift in diffraction angle is assigned to the strong interfacial interaction between the nanoparticles and the elastomeric chain. In order to obtain more structural information, the average crystallite size of ZnS nanoparticles in the composite is calculated from corresponding XRD data and the average size is 16.4 nm.

Scanning electron microscopy (SEM)

The morphological studies of SBR and SBR with different contents of ZnS nanoparticles are analysed by SEM and given in Fig. 2. The SEM image of SBR (Fig. 2a) presents a smooth and homogeneous structure. However, the inclusion of nanoparticles into the

SBR matrix changes the surface morphology of the elastomer composite. From Fig. 2b, it is clear that the sample with 7 phr of ZnS particles containing SBR shows a uniform structure with several nanoparticles which are uniformly distributed. The change in the structural morphology of the composite is attributed to the strong interfacial interaction of the SBR phase with the nanoparticles. However, the surface morphology of the elastomeric composite drastically changes at 15 phr loading of ZnS and shows some agglomeration of nanoparticles in the matrix.

However, at higher loading of nanoparticles (15 phr), it is necessary to point out that the surface morphology of nanocomposite is remarkably changed into a cluster or aggregated structure (Fig. 2c).

Thermogravimetric analysis (TGA)

The thermal stability of SBR and SBR/ZnS nanocomposites at a heating rate of $10^\circ\text{C min}^{-1}$ is shown in Fig. 3. From the figure, it can be seen that all samples show single-step degradation. The initial degradation of SBR is at 401°C which ends around 491°C . The improved thermal stability of SBR/ZnS nanocomposites is clear from the initial and final temperature of the thermograms. The increasing thermal stability of the nanocomposites with the increase in the concentration of nanoparticle is due to the improvement in interfacial adhesion between the ZnS nanoparticles and the elastomeric chain. The nanoparticles with a large surface area can strongly reinforce the SBR matrix, producing a protective layer on the surface of SBR which thereby acquire more thermal stability. The char residue remaining at 600°C is 9.61% for the unfilled SBR. However, for the composites with 5, 10 and 15 phr of nano-ZnS-filled SBR, the values are 14.62, 18.68 and 22.94%, respectively, at 600°C . The char layers act as a protective coating on the surface of the nanocomposite, which prevents further burning. The higher char residue is an indication of the better thermal and flame resistance of the polymer matrix [25]. This, in fact, broadens the utility of these materials in various applications.

Cure characteristics

The effect of loadings of ZnS nanoparticles on the rheometer processing characteristics such as cure time and torque values of SBR is presented in

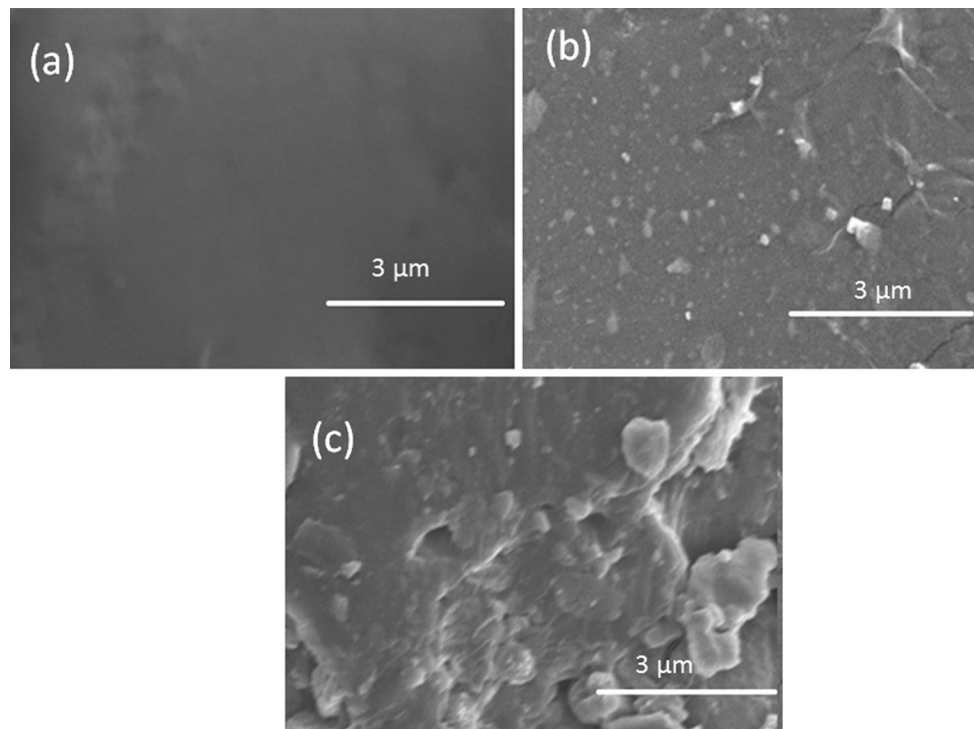


Figure 2 SEM pictures of **a** SBR, **b** SBR with 7 phr and **c** SBR with 15 phr ZnS nanoparticles.

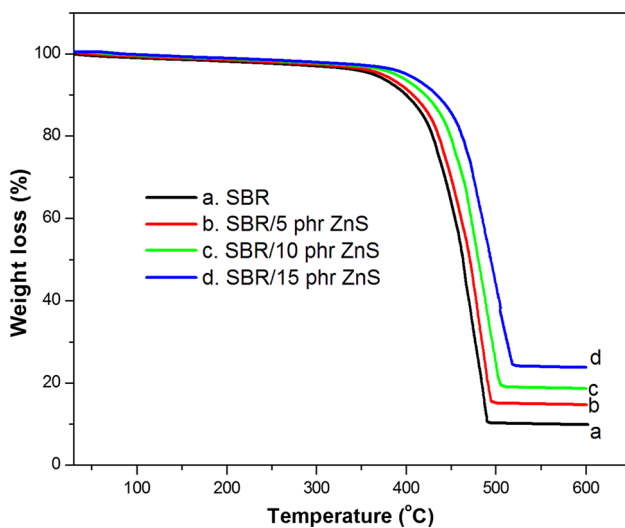


Figure 3 TGA curves of SBR and SBR with different contents of ZnS nanoparticles.

Table 1. The scorch time and optimum cure time values decrease with the loading of ZnS nanoparticles in SBR. This shows that the rate of the curing of SBR increases with the addition of nanoparticles. This is advantageous because it can enhance the production rate of elastomer products developed from these materials. As shown in Table 1, the addition of nanoparticles significantly increases the minimum

and maximum torque values. The increase in rheometric torque indicates a better polymer–filler interaction. Here, the metal sulphide acts as co-activators during the chemical vulcanization process, creating better linkages between the molecular chains of rubber by sulphur, which ultimately leads to the increase in cross-linking. The composite with 10 phr ZnS shows the maximum torque value, and beyond 10 phr loading, the torque value is found to decrease. At higher loading, greater stress develops in the elastomeric matrix which leads to poor cross-links between the polymer and ZnS nanoparticles [26].

Mechanical properties

The mechanical properties of SBR nanocomposites, namely tensile strength, modulus, elongation at break, tear resistance, hardness, abrasion loss, heat build-up and compression set, were determined for all nanofiller loadings. The tensile strength, modulus (at 200% elongation) and tear resistance values are greater than those of pure SBR (Table 2). The variation in the tensile property of composite is more pronounced in 10 phr loading. This means primarily that the nano-ZnS filler acts as a reinforcing filler in SBR and secondarily that there is a homogeneous

Table 1 Processing characteristics of SBR and SBR with different loadings of ZnS nanoparticles

Sample code	Cure time, t_{90} (min)	Scorch time, t_2 (min)	Maximum torque (dNm)	Minimum torque (dNm)
SZ ₀	15.7	4.8	29	6.9
SZ ₃	15.3	4.6	32	7.5
SZ ₅	14.6	4.32	35	7.9
SZ ₇	14.1	4.05	37	8.0
SZ ₁₀	12.8	3.83	40	8.2
SZ ₁₅	12.3	3.55	38	8.1

Table 2 Mechanical properties of SBR and SBR with various contents of ZnS nanoparticles

Properties	Loading of ZnS nanoparticles (phr)					
	0	3	5	7	10	15
Tensile strength (MPa)	2.13	3.87	4.65	5.94	7.19	6.63
Elongation at break (%)	425	419	407	390	381	363
Modulus (300%)	1.94	2.94	4.21	5.19	6.99	5.88
Tear strength (kN m^{-1})	18	23	26	29	32	30
Hardness (Shore-A)	33	34	35	36	38	40
Heat build-up ($^{\circ}\text{C}$)	10	10.5	11.9	12.8	14.3	15.8
Compression set (%)	19.8	19.2	18.32	17.44	16.9	16.3
Abrasion loss (mm^3)	66.8	66.6	66.3	66.0	65.5	65.2

dispersion of nanoparticles in the polymer matrix [27]. The slight decrease in tensile strength, modulus and tear strength observed at higher loadings (15 phr) may be due to the agglomeration of ZnS nanoparticles. The elongation at break (EB) given in Table 2 shows that the EB decreases with the loading of nanoparticles in all cases and it is well known that the decrease in EB is an indication of higher reinforcement by nanoparticles [28]. Durometer hardness is one of the most commonly used hardness tests for elastomeric materials; it assesses the material resistance to indentation and is widely employed in the elastomer industry. The hardness of the nanocomposite vulcanizates at different filler loadings is shown in Table 2. An increase in the hardness of composite can be seen with the increase in the content of ZnS nanoparticles, which is again due to the better interaction between SBR matrix and the nanofiller. Abrasion resistance is the ability of a material to resist the rubbing, scraping or erosion that tends to progressively remove material from its surface. The abrasion resistance of SBR vulcanizate with the various loadings of nanoparticles is also given in Table 2. The abrasion resistance of the composites increased with an increase in the content of nanoparticles up to 10 phr loading. The voids or

cracks at the growing tip of flaw are arrested by the nanosized crystalline ZnS particles, which increase the abrasion resistance. The decrease in abrasion resistance beyond 10 phr loading of ZnS can be attributed to the poor interfacial interaction between SBR and the nanoparticles resulting from agglomeration of ZnS. The compression set measurement is used to measure the ability of an elastomeric material to maintain the elastic properties even after prolonged compressive stress. Table 2 shows the compression set values of the SBR vulcanizate with different loadings of ZnS nanoparticles. Pure SBR has higher compression set values than nanocomposites, and on increasing filler loading the compression set values decrease. It is noteworthy here that a lower compression set is the key property for the rubber industry in sealing applications. Heat build-up is another important property of elastomers, arising from the internal friction in the compounds. From Table 2, it is clear that the heat build-up of the elastomeric composites enhances with the amount of ZnS nanoparticles and this is mainly due to the higher internal friction resulting from more extensive cross-linking and improved thermal conductivity of the nanocomposites. The magnitude of the increase in heat build-up is higher at 15 phr ZnS loading. The

reinforcing effect and higher thermal conductivity of metal sulphide-filled compounds are responsible for the high heat build-up value.

AC conductivity

The AC conductivity of various concentrations of nano-ZnS-filled SBR and unfilled SBR at different frequencies is given in Fig. 4. The SBR shows minimum electrical conductivity compared to that of the metal sulphide nanoparticles-filled SBR. Due to the highly amorphous nature of SBR (confirmed from XRD analysis), the macromolecular chains are randomly oriented in the SBR matrix. Therefore, the linkages through grain boundaries are poor, leading to a lower electrical conductivity of the elastomer. The AC conductivity increases continuously with an increase in frequencies for all the samples. This is due to the rapid transport of hopping charge carriers within the polymer matrix and its composites. From the figure, it can be seen that the AC conductivity of the composite greatly increased with the addition of nanoparticles, and the composite with 10 phr filler shows the maximum AC conductivity. This indicates the strong interfacial interactions between the ZnS nanoparticles and the SBR matrix. The interfacial interaction changes the molecular orientation of SBR from a randomly oriented conformation to a well-defined compact structure. It is well recognized that the bulk conductivity of nanocomposites depends on the loading of fillers, filler–rubber adhesion and uniform dispersion of nanoparticles within the

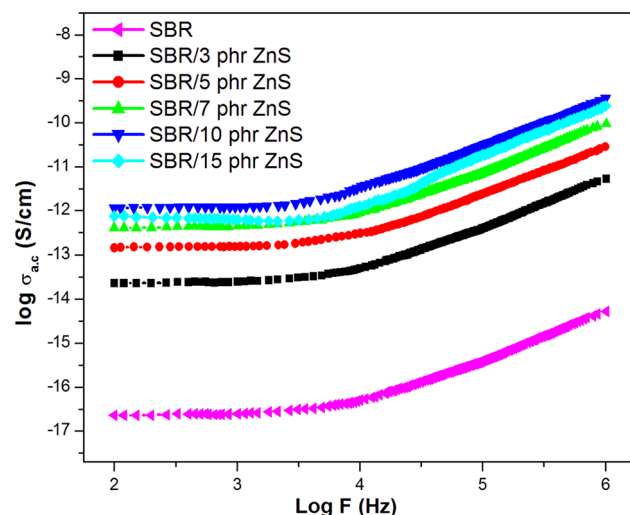


Figure 4 AC conductivity of SBR and SBR with different contents of ZnS nanoparticles.

polymer matrix [29]. However, the interfacial adhesion between the polymer and filler decreases at higher concentration of nanoparticles (15 phr) which is due to the high tendency of nanoparticles for aggregation. This breaks the formation of effective conducting chains of ZnS nanoparticles, and therefore the conductivity is lower at a higher concentration of nanoparticles.

Dielectric loss ($\tan \delta$)

Dielectric loss tangent ($\tan \delta$) is the ratio of the electrical energy dissipated in a material to the total power in a circuit. Figure 5 shows the variation in the dielectric loss tangent ($\tan \delta$) as a function of frequency ranging from 100 to 10^6 Hz of SBR and SBR/ZnS nanocomposites at room temperature. It is observed that the $\tan \delta$ of the composite is higher than that of pure SBR. It is evident that the dielectric loss of all the samples decreases steadily with the frequency and reaches a constant $\tan \delta$ value at 10^4 Hz. This is due to the time lag associated with the orientation of dipoles within the polymer matrix. The nanoparticles present in the macromolecular chain of SBR increase the interactions between the components, leading to field distortions and thus an increase in dielectric loss. It is interesting to observe from the figure that the composite with 10 phr ZnS shows the higher dielectric loss, which might be due to the large surface area, surface domain polarization and the effective electrical network formation [30].

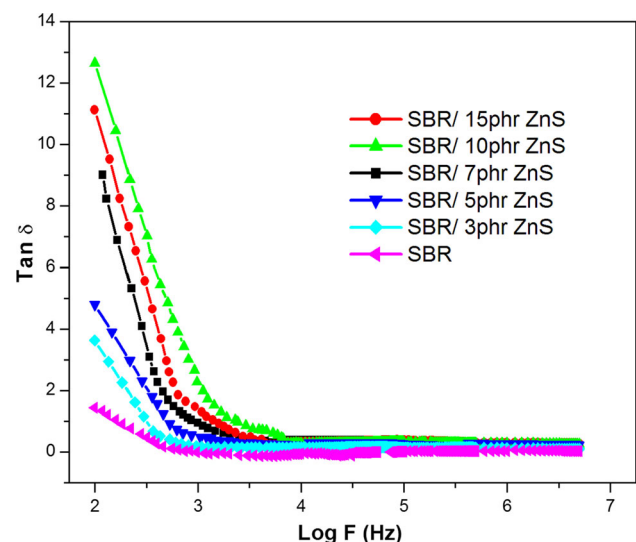


Figure 5 Dielectric loss tangent of SBR and different contents of nano-ZnS-filled SBR.

The dielectric loss of the 15 phr loading is lower than that of 10 phr loaded composite. This is due to the formation of clusters or discrete aggregates in the SBR matrix, which prevents charge carriers from migrating through the elastomeric system.

Diffusion studies

Effect of loading on sorption

The results of sorption experiments were obtained as moles of solvent uptake by 100 g of polymer sample (Q_t mol%) [31]

$$Q_t \text{ (mol\%)} = \frac{\text{Mass of solvent sorbed/Molar mass of solvent}}{\text{Mass of polymer}} \times 100 \tag{1}$$

The uptake of petrol through SBR and SBR with ZnS nanoparticles vulcanizates at room temperature is shown in Fig. 6. It can be seen that the mol% uptake of the SBR samples decreases with the increasing concentration of ZnS. The equilibrium solvent uptake is lowest for the composite sample with 10 phr filler, while the highest value is for unfilled SBR vulcanizates. All the compounds show similar sigmoidal trend in all the solvents. The activation energy required for the diffusion process is higher for large penetrant molecules. The diffusion rate is directly related to the ease with which the polymer segments exchange their position to create free volume inside the matrix, in accordance with free volume theory [31]. There is more space required for the progressive diffusion of large penetrant molecules, and this makes the diffusion process more difficult. Thus, in the case of ZnS-filled SBR matrix, the exchange process becomes more tedious.

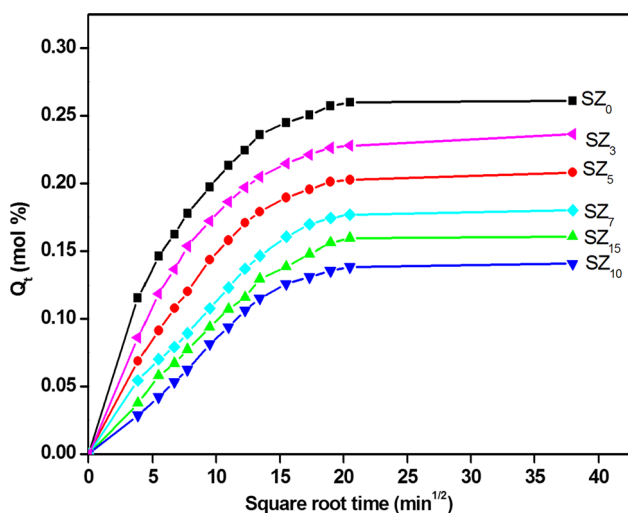


Figure 6 Sorption curves of various contents of nano-ZnS-filled SBR composite through petrol at room temperature (SZ_0 is SBR, SZ_3 , SZ_5 , SZ_7 , SZ_{10} and SZ_{15} are 3, 5, 10 and 15 phr of ZnS/SBR nanocomposites).

nanoparticles and the SBR matrix. Reinforcement in polymer composites leads to a restriction in polymer segmental mobility, which increases the solvent resistance. Also, this can be due to a better distribution of nanoparticles in the composite. Upon further loading of nanoparticles (15 phr ZnS), mole uptake increases due to the poor polymer–filler interaction resulting from the agglomeration of nanoparticles in the matrix.

Effect of penetrant size on mole uptake

Figure 7 shows the sorption curves of SBR with 10 phr ZnS composite in different industrial solvents such as petrol, kerosene and diesel. The mol% uptake decreases with an increase in molecular weight of solvents. Petrol exhibits higher sorption, diesel the lowest, while kerosene shows the intermediate value. All the composites show a similar sigmoidal trend in all the solvents. The activation energy required for the diffusion process is higher for large penetrant molecules. The diffusion rate is directly related to the ease with which the polymer segments exchange their position to create free volume inside the matrix, in accordance with free volume theory [31]. There is more space required for the progressive diffusion of large penetrant molecules, and this makes the diffusion process more difficult. Thus, in the case of ZnS-filled SBR matrix, the exchange process becomes more tedious.

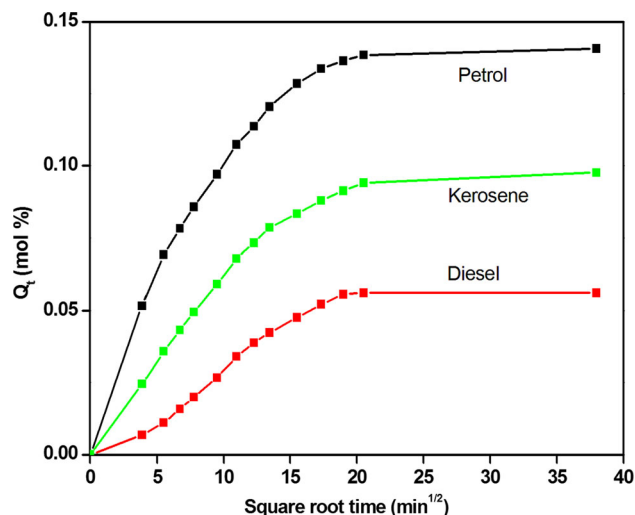


Figure 7 Solvent uptake of SBR with 10 phr of ZnS in different industrial solvents (petrol, kerosene and diesel).

Effect of temperature on mole uptake

Figure 8 shows the mol% uptake of SBR/ZnS in petrol at three different temperatures (27, 40 and 50 °C). Here, we selected the sample with 10 phr ZnS loading because of its high solvent resistance at room temperature. It is observed that the diffusion rate and solvent uptake increase with an increase in the temperature. This is due to the higher free volume generated in the polymer chain; also, the increase in segmental mobility again improves the kinetic energy of the polymer chains, causing the increased collision of particles in the matrix [32]. From the plots, it is clear that all the plots of Q_t versus \sqrt{t} are sigmoidal and are temperature dependent also.

Diffusion (D), sorption (S) and permeation (P) coefficients

The diffusion coefficient (D) is a kinetic parameter. On the basis of segmental mobility, D controls diffusion rate. It is calculated using the equation

$$D = \pi \left(\frac{h\theta}{4Q_\infty} \right)^2 \quad (2)$$

where h is the thickness of the sample, θ is the slope of the initial linear region of the plot of Q_t versus the square-root time, and Q_∞ is the equilibrium mol uptake. The D values (Table 3) decrease with an increase in the concentration of ZnS nanoparticles up to 10 phr loading. The lowest value of diffusion coefficient is observed for SBR sample containing

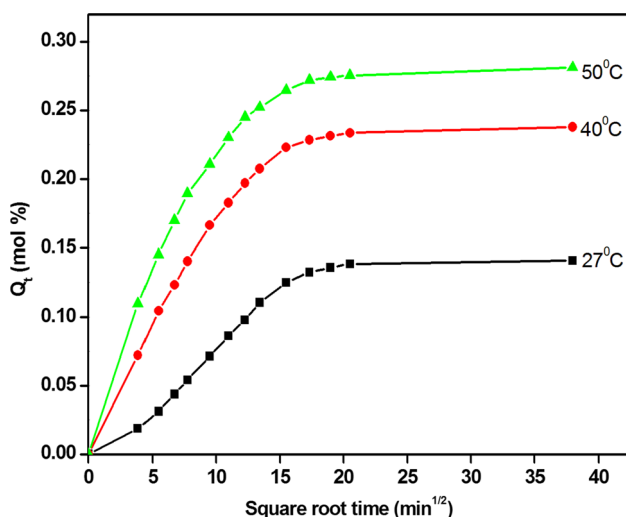


Figure 8 Mole uptake of SBR and SBR with 10 phr of ZnS in petrol at 27, 50 and 70 °C.

10 phr ZnS. This is due to the strong interfacial adhesion between the elastomer and nanoparticles. However, the D value of 15 phr sample is higher than the 10 phr ZnS containing SBR. This is because of the agglomeration of nanoparticles. Such agglomerations result in non-uniform distribution of ZnS nanoparticles in the polymer matrix. As the penetrant size increases, diffusivity decreases; petrol shows the highest D value and diesel shows the lowest. This is explained on the basis of the free volume theory [31] in terms of the effect of solvent on the mol% uptake of solvent.

The study reveals that the sorption, diffusion and permeation coefficients are highest for petrol, lowest for diesel and intermediate for kerosene. Due to the steric reason, the smaller molecules will diffuse and get accommodated more easily into the polymer matrix. The decrease in sorption values of composites with the increase in nanofiller loading can be explained by the reinforcing phenomenon in SBR caused by ZnS nanoparticles. The reinforcement creates obstacles for the penetrating molecules. The bigger the penetrant molecule, the stronger the resistance and hence less will be the penetrant uptake. The permeation coefficient is the combined effect of the diffusion and sorption coefficients, i.e. $P = D \cdot S$, which is the measure of the amount of solvent that permeated per unit area of the sample in one second. The permeation coefficient shows a trend similar to that of D and S .

Mechanism of transport

From the swelling data, the mechanism of transport is calculated by the following equation

$$\log \frac{Q_t}{Q_\infty} = \log k + n \log t \quad (3)$$

where Q_t and Q_∞ are the mol% sorption at time t and at equilibrium, respectively, n represents the mode of transport, and k indicates the interaction between the polymer and the penetrant. The values of n and k are given in Table 4. If the value of n is 0.5, the mechanism of transport is Fickian. The diffusion rate of solvent penetrant into the matrix remains very low as compared to the rate of relaxation of the polymer chains. When $n = 1$, the mode of transport is said to be non-Fickian, which means that the rate of diffusion and the relaxation process is opposite to that of the Fickian mode of transport [33]. There is another

Table 3 *D*, *S* and *P* values of SBR/ZnS nanocomposites in various industrial solvents

Samples	Diffusion coefficient <i>D</i> × 10 ⁵ (cm ² s ⁻¹)			Sorption coefficient <i>S</i> (mol%)			Permeation coefficient <i>P</i> × 10 ⁵ (cm ² s ⁻¹)		
	Petrol	Kerosene	Diesel	Petrol	Kerosene	Diesel	Petrol	Kerosene	Diesel
SZ ₀	1.51	1.36	1.25	1.21	1.17	1.14	1.81	1.59	1.42
SZ ₃	1.38	1.24	1.18	1.19	1.13	1.11	1.64	1.40	1.31
SZ ₅	1.34	1.18	1.13	1.11	1.07	1.06	1.48	1.26	1.19
SZ ₇	1.19	1.13	1.11	1.09	1.03	1.01	1.29	1.16	1.12
SZ ₁₀	1.11	0.94	0.88	1.01	0.92	0.88	1.21	0.86	0.77
SZ ₁₅	1.14	1.06	1.03	1.07	0.98	0.95	1.22	1.03	0.97

Table 4 *n* and *k* values of SBR/ZnS with composites in industrial solvents at room temperature

Samples	Petrol		Kerosene		Diesel	
	<i>n</i>	<i>K</i> × 10 ² (min ⁻¹)	<i>n</i>	<i>k</i> × 10 ² (min ⁻¹)	<i>n</i>	<i>K</i> × 10 ² (min ⁻¹)
SZ ₀	0.37	0.28	0.49	0.26	0.52	0.22
SZ ₃	0.45	0.29	0.56	0.24	0.66	0.21
SZ ₅	0.67	0.21	0.62	0.19	0.68	0.17
SZ ₇	0.69	0.19	0.66	0.16	0.71	0.14
SZ ₁₀	0.77	0.13	0.79	0.12	0.83	0.11
SZ ₁₅	0.75	0.15	0.66	0.17	0.72	0.12

mode of transport, known as anomalous, in which the value of *n* is in between 0.5 and 1. This means that the rate of relaxation of the polymer matrix and the rate of diffusion of the penetrant molecule are almost the same. From Table 4, it is clear that the value of *n* increases with the increase in loading of ZnS nanoparticles. It is also seen that the value of *n* increases with an increase in molecular weight of solvents. Here, the composites show an anomalous mode of transport and at higher filler loading the value of *n* is nearer to non-Fickian. This indicates the better interfacial adhesion between filler and the polymer matrix. The structural property of polymeric materials is well clear from the *k* values. More specifically, the *k* values give an idea about the interaction of the polymer with the solvent molecules. The *k* value decreases with the loading of ZnS nanoparticles in SBR matrix, and this is another evidence for the strong interfacial interaction between nanofiller and the elastomer.

Activation energy of sorption and permeation

The activation energy of sorption (*E_D*) and permeation (*E_P*) can be obtained from *D* and *P* values at different temperatures, calculated from the Arrhenius equation

$$X = X_0 e^{-E_x/RT} \tag{4}$$

where *X* is *P* or *D*, *X₀* is *P₀* or *D₀*, and *E* is the activation energy obtained by plotting log *D* versus 1/*T* and log *P* versus 1/*T*. The activation energy for diffusion (*E_D*) and the activation energy for permeation (*E_P*) are shown in Table 5. The activation energy of diffusion and permeation of composites in different industrial solvents increases with an increase in filler concentration. It also is seen that the activation energy parameter of composites increases with the increase in molecular mass of solvent. Petrol shows the least and diesel shows minimum activation energy. This is in good agreement with our previous work reported earlier [34] which points out the role of steric effect of penetrant molecules in the diffusion and transport processes. The composite with 10 phr ZnS shows the maximum activation energy value indicating the better distribution of nanoparticles in the SBR matrix. The difference between *E_P* and *E_D* will give the enthalpy of sorption (*ΔH*). The enthalpy of sorption also shows a similar trend and is found to be in endothermic also.

Thermodynamic parameters

From the Van't Hoff's relation, thermodynamic parameters can be obtained,

Table 5 E_D and E_P (kJ mol^{-1}) values of SBR/ZnS nanocomposites in various industrial solvents

Samples	Petrol			Kerosene			Diesel		
	E_D	E_P	ΔH	E_D	E_P	ΔH	E_D	E_P	ΔH
SZ ₀	3.59	4.22	0.63	3.97	4.72	0.75	4.62	5.46	0.84
SZ ₃	4.49	5.41	0.92	4.54	5.65	1.11	4.63	6.15	1.52
SZ ₅	5.92	7.07	1.15	6.18	7.44	1.26	7.08	8.89	1.81
SZ ₇	6.08	7.29	1.21	6.32	7.69	1.37	7.19	9.09	1.9
SZ ₁₀	6.29	7.54	1.25	6.49	8.36	1.87	7.59	9.64	2.05
SZ ₁₅	6.16	7.39	1.23	6.39	7.88	1.49	7.29	9.23	1.94

Table 6 ΔH , ΔS and ΔG (kJ mol^{-1}) values of SBR/ZnS nanocomposites in industrial solvents

Samples	ΔH			ΔS			$-\Delta G$		
	Petrol	Kerosene	Diesel	Petrol	Kerosene	Diesel	Petrol	Kerosene	Diesel
SZ ₀	0.635	0.758	0.848	0.068	0.048	0.042	19.77	13.64	11.752
SZ ₃	0.927	1.117	1.527	0.058	0.044	0.039	16.47	12.08	10.173
SZ ₅	1.158	1.268	1.817	0.047	0.032	0.029	12.94	8.332	6.883
SZ ₇	1.217	1.378	1.979	0.043	0.029	0.022	11.68	7.322	4.621
SZ ₁₀	1.258	1.879	2.059	0.029	0.024	0.014	7.44	5.321	2.141
SZ ₁₅	1.239	1.497	1.946	0.037	0.026	0.017	9.86	6.303	3.154

$$\log K_s = \frac{\Delta S_s}{2.303R} - \frac{\Delta H_s}{2.303RT} \quad (5)$$

where K_s is the equilibrium constant; it is the ratio of the number of moles of solvent sorbed at equilibrium to the sample initial mass. The change in enthalpy and entropy can be calculated by plotting $\log K_s$ versus $1/T$. The thermodynamic properties of the polymer and its nanocomposites in petroleum fuels are given in Table 6. It can be seen that the enthalpy change of all the samples increases with the increasing concentration of filler. Upon moving from petrol to diesel, the ΔH values also increase, which is in accordance with Henry's law. The entropy change values (ΔS) are found to be positive, and it decreases with increase in the concentration of ZnS. The increased interfacial interaction between matrix and filler results in the reduction in entropy change [35]. The negative ΔG values are decreased from unfilled SBR to the ZnS-filled SBR; 10 phr filler containing the composite shows a minimum ΔG value. Thus, in pure SBR spontaneous sorption occurs and SBR/10 phr ZnS has minimum spontaneity in the diffusion process. All the thermodynamic values indicate the better interaction between the nanofiller and the SBR matrix.

Conclusions

This work reported the processability, mechanical properties, thermal stability, electrical conductivity and transport behaviour of SBR and SBR/ZnS nanocomposites. The compounded SBR/ZnS samples indicated higher production rate due to the lower cure time of composites. The incorporation of ZnS nanoparticles into polymer matrix reduces the amorphous nature of SBR. There was the regular improvement in mechanical properties of composites up to 10 phr loading of ZnS. The magnitude of mechanical performance dropped with the further addition of ZnS in SBR. Mechanical properties such as tensile, tear strength, modulus, hardness, abrasion resistance, heat build-up and compression set were in agreement with the reinforcement by ZnS particles. This is advantageous because the elastomer nanocomposites with improved mechanical properties tend to perform better and more durable in service life. The observed mechanical properties were also supported by the filler distribution and reinforcement revealed by SEM and diffusion studies. The AC conductivity of SBR was significantly enhanced with the addition of ZnS nanoparticles. The diffusivity of solvent through the nanocomposite was lower, due to the higher reinforcement of nanoparticles. The activation parameter and sorption

coefficient showed a dependence on the size of penetrant molecules. Thus, it can be concluded that nano-ZnS acts as a good reinforcement for SBR, especially at 10 phr loading.

Acknowledgements

The authors wish to thank Prof. P. P. Pradyumnan, Department of Physics, University of Calicut, for providing necessary facilities in the department.

Compliance with ethical standards

Conflict of interest The authors of this article have no conflict of interest to declare.

References

- [1] Maria HJ, Lyczko N, Nzihou A, Mathew C, George SC, Joseph K, Thomas S (2013) Transport of organic solvents through natural rubber/nitrile rubber/organically modified montmorillonite nanocomposites. *J Mater Sci* 48:5373–5386. <https://doi.org/10.1007/s10853-013-7332-7>
- [2] Li Y, Wang Q, Wang T, Pan G (2012) Preparation and tribological properties of graphene oxide/nitrile rubber nanocomposites. *J Mater Sci* 47:730–738. <https://doi.org/10.1007/s10853-011-5846-4>
- [3] Liu Q, Zhang Y, Xu H (2008) Properties of vulcanized rubber nanocomposites filled with nanokaolin and precipitated silica. *Appl Clay Sci* 42:232–237
- [4] Kar S, Maji PK, Bhowmick AK (2010) Chlorinated polyethylene nanocomposites: thermal and mechanical behavior. *J Mater Sci* 45:64–71. <https://doi.org/10.1007/s10853-009-3891-z>
- [5] Jasna VC, Ramesan MT (2017) Studies on the mechanical, electrical properties and interaction of petroleum fuels with SBR/manganous tungstate nanocomposites. *J Inorg Organomet Polym Mater* 27:968–978
- [6] Jacob M, Varughese KT, Thomas S (2006) Dielectric characteristics of sisal–oil palm hybrid biofibre reinforced natural rubber biocomposites. *J Mater Sci* 41:5538–5547. <https://doi.org/10.1007/s10853-006-0298-y>
- [7] Ismail H, Salleh SZ, Ahmad Z (2013) Fatigue and hysteresis behavior of halloysite nanotubes-filled natural rubber (SMR L and ENR 50) nanocomposites. *J Appl Polym Sci* 127:3047–3052
- [8] Meera AP, Thomas PS, Thomas S (2012) Effect of organoclay on the gas barrier properties of natural rubber nanocomposites. *Polym Compos* 33:524–531
- [9] Pazhooh HN, Bagheri R, Adloo A (2017) Fabrication of semi-conductive natural rubber nanocomposites with low copper nanoparticle contents. *Polymer* 108:135–145
- [10] Suhailath K, Ramesan MT (2017) Temperature dependent AC conductivity, mechanical and different DC conductivity modeling of poly (butyl methacrylate)/samarium doped titanium dioxide nanocomposites. *J Mater Sci: Mater Electron* 28:13797–13805
- [11] Basuli U, Chattopadhyay S, Nah C, Chaki TK (2012) Electrical properties and electromagnetic interference shielding effectiveness of multiwalled carbon nanotubes-reinforced EMA nanocomposites. *Polym Compos* 33:897–903
- [12] Jayakrishnan P, Ramesan MT (2017) Synthesis, structural, magnetoelectric and thermal properties of poly (anthranilic acid)/magnetite nanocomposites. *Polym Bull* 74:3179–3198
- [13] Seentrakoon B, Junhasavasdikul B, Chavasiri W (2013) Enhanced UV-protection and antibacterial properties of natural rubber/rutile-TiO₂ nanocomposites. *Polym Degrad Stab* 98:566–578
- [14] Jiang MJ, Dang ZM, Xu HP (2007) Enhanced electrical conductivity in chemically modified carbon nanotube/methylvinyl silicone rubber nanocomposite. *Eur Polym J* 43:4924–4930
- [15] Ramesan MT, Nidhisha V, Jayakrishnan P (2017) Synthesis, characterization and conducting properties of novel poly (vinyl cinnamate)/zinc oxide nanocomposites via in situ polymerization. *Mater Sci Semicond Process* 63:253–260
- [16] Jia Z, Xu T, Yang S, Luo Y, Jia D (2014) Interfacial mechano-chemical grafting in styrene–butadiene rubber/halloysite nanotubes composites. *Polym Test* 54:29–39
- [17] Ramesan MT (2014) Effect of fly ash on thermal stability, flammability, oil resistance and transport properties of chlorinated styrene butadiene rubber composites. *J Elastomers Plast* 46:303–324
- [18] Abraham J, Maria HJ, George SC, Kalarikkal N, Thomas S (2015) Transport characteristics of organic solvents through carbon nanotube filled styrene butadiene rubber nanocomposites: the influence of rubber–filler interaction, the degree of reinforcement and morphology. *Phys Chem Chem Phys* 17:11217–11228
- [19] Kumar PVA, Kumar SA, Varughese KT, Thomas S (2012) Transport properties of high-density polyethylene/ethylene propylene diene terpolymer blends. *J Mater Sci* 47:3293–3304. <https://doi.org/10.1007/s10853-011-6168-2>
- [20] Donald IW, Mallinson PM, Metcalfe BL (2011) Recent developments in the preparation, characterization and applications of glass- and glass–ceramic-to-metal seals and coatings. *J Mater Sci* 46:1975–2000. <https://doi.org/10.1007/s10853-010-5095-y>

- [21] Gong FL, Zhao CG, Feng M, Qin HL, Yang MS (2004) Synthesis and characterization of PVC/montmorillonite nanocomposite. *J Mater Sci* 39:293–294. <https://doi.org/10.1023/B:JMSC.0000007758.00802.1a>
- [22] Zheng JP, Wang JX, Gao S, Yao KD (2005) Synthesis and characterization of PMMA/montmorillonite nanocomposites by emulsion polymerization. *J Mater Sci* 40:4687–4689. <https://doi.org/10.1007/s10853-005-3928-x>
- [23] Ramesan MT, Nihmath A, Francis J (2013) Preparation and characterization of zinc sulphide nanocomposites based on acrylonitrile butadiene rubber. *AIP Conf Proc* 1536:255–257
- [24] Al Stroyuk, Raevskaya AE, Korzhak AV, Kuchmii SY (2007) Zinc sulfide nanoparticles: spectral properties and photocatalytic activity in metals reduction reactions. *J Nanopart Res* 9:1027–1039
- [25] Sampreeth T, Al-Maghrabi MA, Bahuleyan B, Ramesan MT (2018) Synthesis, characterization, thermal properties, conductivity and sensor application study of polyaniline/cerium doped titanium dioxide nanocomposites. *J Mater Sci* 53:591–603. <https://doi.org/10.1007/s10853-017-1505-8>
- [26] Jasna VC, Ramesan MT (2017) Preparation, characterization, dielectric properties and diffusion studies of styrene butadiene rubber (SBR)/manganous tungstate ($MnWO_4$) nanocomposites. *AIP Conf Proc* 1849:20044–20056
- [27] Johnson T, Thomas S (2000) Effect of epoxidation on the transport behaviour and mechanical properties of natural rubber. *Polymer* 41:7511–7522
- [28] Ramesan MT (2015) Effects of magnetite nanoparticles on morphology, processability, diffusion and transport behavior of ethyl vinyl acetate nanocomposites. *Int J Plast Technol* 19:368–380
- [29] Ramesan MT, Surya K (2017) Fabrication of biopolymer nanocomposite from natural resource materials. *Polym Compos* 38:E66–E73
- [30] Nihmath A, Ramesan MT (2017) Fabrication, characterization and dielectric studies of NBR/hydroxyapatite nanocomposites. *J Inorg Organomet Polym* 27:481–489
- [31] Sareena C, Ramesan MT, Purushothan E (2013) Transport studies of peanut Shell powder reinforced natural rubber composites in chlorinated solvent. *Fibers Polym* 14:1674–1687
- [32] Sen SK, Dasgupta B, Banerjee S (2009) Effect of introduction of heterocyclic moieties into polymer backbone on gas transport properties of fluorinated poly(ether imide) membranes. *J Membr Sci* 343:97–103
- [33] Mathai AE, Singh RP, Thomas S (2002) Transport of substituted benzenes through nitrile rubber/natural rubber blend membranes. *J Membr Sci* 202:35–54
- [34] Sareena C, Sreejith MP, Ramesan MT, Purushothaman E (2015) Transport properties of coconut shell powder (CSP)-reinforced natural rubber composites in aromatic solvents. *Polym Bull* 72:1683–1702
- [35] Padhi S, Achary PGR, Nayak NC (2015) Molecular transport behaviour of organic solvents through halloysite nanotubes filled ethylene-vinyl acetate copolymer. *Bull Mater Sci* 38:925–933